

## High-strength RC columns subjected to high-axial and increasing cyclic lateral loads

Muhammad Y. Bhayusukma\* and and Keh-Chyuan Tsai<sup>a</sup>

Department of Civil Engineering, National Taiwan University,  
No. 1, Sec. 4, Roosevelt Road, Taipei, Taiwan

(Received December 24, 2013, Revised March 22, 2014, Accepted March 29, 2014)

**Abstract.** This experimental investigation was conducted to examine the behavior and response of high-strength material (HSM) reinforced concrete (RC) columns under combined high-axial and cyclic-increasing lateral loads. All the columns use high-strength concrete ( $f_c' = 100$  MPa) and high-yield strength steel ( $f_y = 685$  MPa and  $f_y = 785$  MPa) for both longitudinal and transverse reinforcements. A total of four full-scale HSM columns with amount of transverse reinforcement equal to 100% more than that required by earthquake resistant design provisions of ACI-318 were tested. The key differences among those four columns are the spacing and configuration of transverse reinforcements. Two different constant axial loads, i.e. 60% and 30% of column axial load capacity, were combined with cyclically-increasing lateral loads to impose reversed curvatures in the columns. Test results show that columns under 30% of axial load capacity behaved much more ductile and had higher lateral deformational capacity compared to columns under the 60% of axial load capacity. The columns using closer transverse reinforcement spacing have slightly higher ductility than columns with larger spacing.

**Keywords:** high-strength concrete; high-yield strength steel; high-axial load, RC column, cyclic loads, ductility

### 1. Introduction

In recent years, the use of high-strength concrete (HSC) for reinforced concrete (RC) constructions has been widely adopted due to its advantages (Legeron and Paultre 2000; Hwang and Yun 2003; Hwang *et al.* 2005; Xiao *et al.* 2008). Among those, reducing in member size and self-weight and increasing lateral stiffness due to excellent mechanical properties are some of the key ones. The development of the concrete technology, such as self-compacting and fiber-added RC, also accelerated the use of HSC as the primary building construction material (Kawai 2007; Ashtiani, *et al.* 2013). Today, concrete with a compressive strength up to 100 MPa is readily available in the market. On the other hand, over inflated cost of the land in the metropolitan cities has forced the building owner to use high quality construction material, such as HSC, in order to reduce the construction cost and increase the usable floor areas in the building. HSC will reduce the required

---

\*Corresponding author, Ph.D. Candidate, E-mail: muhammadyani05@yahoo.com

<sup>a</sup>Professor

space whenever the structural members use the concrete for axial load-dominated resistance (Rashid *et al.* 2002; Li and Park 2004; Zhou *et al.* 2010).

However, in high-seismicity regions, ductility of structures is one of the most essential parameter for structural engineers to consider when they are performing the building design. As widely known, concrete is a brittle material. Consequently, RC high-rise buildings must be designed properly to withstand against strong earthquakes, particularly when they are made from HSC. This is because of HSC much brittle than normal concrete. To resolve this issue, combining HSC with high-yield strength steel for longitudinal and transverse reinforcements has become one of the possible alternatives. It has been confirmed that the performance of RC columns can be significantly improved by using more confining steel (Ho and Luo 2012). The use of high-yield strength stirrups would not only provide good confinement for HSC core but also keep the stirrup to remain elastic for cracks control. Nevertheless, the stirrup spacing could be increased to improve the constructability of RC members (Zhou *et al.* 2010). This alternative material is known as high-strength material (HSM).

Currently, ACI-318 code permits to use steel reinforcement with a yield stress  $f_y$  up to 700 MPa. The use of high-yield strength steel is still restricted except for the confinement reinforcement in compression members (Lepage *et al.* 2008). In addition, existing RC building provisions, such as ACI-318 or CSA-A23.3, have not fully addressed the use of HSM because these materials have relatively short history.

In order to promote the application of HSM to RC members, it is necessary to evaluate the seismic performance of these members. However, the research on full-scale HSM columns is still limited. This limitation is due to the high cost of large scale testing and the availability of large experimental facilities required. For this reason, the investigation of the behavior and responses of four full-scale HSM columns using combined high-axial and cyclically-increasing lateral loads was carried out. The tests were carried out using an advanced testing facility called Multi-Axial Testing System (MATS) in National Centre for Research on Earthquake Engineering (NCREE), Taipei, Taiwan. The detailed experimental results are presented in this paper.

## 2. Research significance

This paper presents the experimental observation and data analysis related to the behavior of full-scale HSM columns subjected to high-axial and cyclically-increasing lateral loads. In the past, most of the studies on HSM columns were based on either relatively small-scale specimens or applying low-axial load. Therefore, the knowledge gained from this research will not only fill the gap on realistic responses of full-scale HSM columns but also increase the data base related to the HSM columns. The results from this research are expected to provide contribution to the development of earthquake resistant design guidelines for HSM structures in the future.

## 3. Experimental program

### 3.1 Specimen design

A total of four full-scale square HSM columns (identified as NRC-A1, NRC-A2, NRC-B1 and

Table 1 Details of the columns

Column	$P/P_0$	Longitudinal reinforcement		Transverse reinforcement			
		Bar No.	$\rho$ (%)	Bar No.	$\rho_t/\rho_{ACI}$	Spacing (mm)	Configuration
NRC-A1	0.6	16#8	2.53	#4	0.99	105	Type A
NRC-A2	0.3	16#8	2.53	#4	0.99	105	Type A
NRC-B1	0.6	16#8	2.53	#4	1.00	120	Type B
NRC-B2	0.3	16#8	2.53	#4	1.00	120	Type B

NRC-B2) were tested using MATS in NCREC. All column cross-sectional dimensions are 600mm×600mm with a clear height of 1800mm. Fig. 1 and Table 1 provide the detail of HSM columns and transverse reinforcement configurations.

The longitudinal reinforcements are 16#8 bars  $A_s = 510 \text{ mm}^2$ , resulting in a reinforcement ratio of 2.53%. The transverse reinforcements are #4 bars  $A_s = 129 \text{ mm}^2$  using two different configurations A and B, all with a reinforcing ratio complying with the ACI-318 provisions. Type A configuration is used for columns NRC-A1 and A2 with a 105mm spacing, while type B configuration is used for columns NRC-B1 and B2 with a 120mm spacing. Those spacings are designed so that the transverse reinforcements provided in all columns are 100% more than that prescribed by the earthquake resistant design provision of ACI-318 (ACI Committee 318, 2011).

Each transverse reinforcement configuration consists of four peripheral hoops arranged in a stack with the 135-degree hook at the end meeting the recommendation of ACI-318. Two different constant axial loads, i.e. 60% (NRC-A1 and B1) and 30% (NRC-A2 and B2) of the column axial-load capacity, were applied simultaneously with cyclically-increasing lateral loads to impose reversed curvatures in the columns. Here, the column axial-load capacity  $P_0$  is taken as  $0.85 f'_c (A_g - A_s) + A_s f_y$ . This strength provision, commonly adopted for the normal strength RC column, holds for high-strength concrete columns as suggested by the ACI Committee 363 on the basis of experimental data (ACI Committee 363 (1992, Reapproved 1997)).

The 60% of column axial load capacity (approximately 23470 kN) has been chosen to represent approximately the maximum axial load level allowed by design codes, as the maximum nominal strength recommended by ACI 318 is  $\phi P_{n(max)} = 0.80\phi P_0 = 0.52P_0$ . This is possible in the base column of a high-rise building constructed using HSM. In this study, applying axial load of  $0.60P_0$  allows the earthquake resisting performance evaluation of HSM columns at a 3.0% radians targeting drift (Elwood *et. al*, 2009). For comparison purposes, an axial load of  $0.30 P_0$  (approximately 11730 kN) was also chosen.

### 3.2 Materials

All four HSM columns were constructed in a precast plant using ready-mix concrete with a specified compressive strength  $f'_c$  equal to 100 MPa. Nine concrete cylinders were cast for each column and tested at 7 and 28-day as well as at the D-day on the test dates. The concrete cylinders were made in either standard case of 150 mm × 300 mm or 100 mm × 200 mm and treated by water-based cured in the precast plant. The choice of 100 mm × 200 mm concrete cylinder was purely to accommodate the maximum capacity of concrete testing machine due to its high strength. When a large-capacity testing machine is needed, test of 7- and 28-day specimens were done in a private

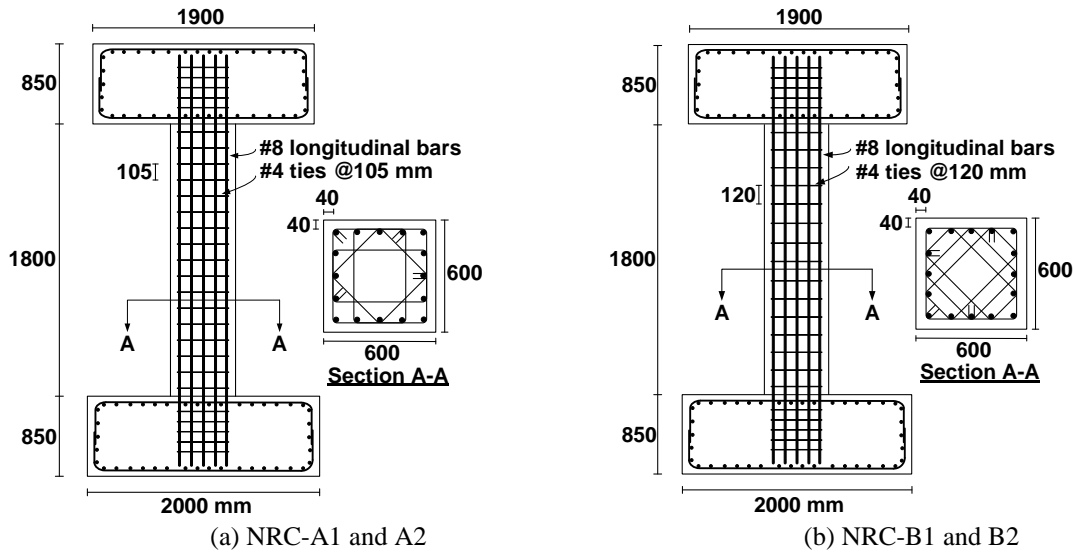


Fig. 1 Specimen details

Table 2 Concrete cylinder test results

Column	Average compressive strength						$E_c$ , MPa at D-day
	Age (days)	$f'_c$ , MPa	Age (days)	$f'_c$ , MPa	at D-day (days)	$f'_c$ , MPa	
NRC-A1	7	56	28	112	62	98	36335
NRC-A2	7	94	28	111	48	106	36944
NRC-B1	7	80	28	108	59	105	40304
NRC-B2	7	100	28	118	37	111	37896

Table 3 Mechanical properties of reinforcing steel

Bar No.	Bar ID	$f_y$ , MPa	$f_u$ , MPa	$\epsilon_y (\times 10^{-2})$	$\epsilon_u (\times 10^{-2})$	Stress Ratio, $\epsilon_u/\epsilon_y$
#8	6225-1	765	1005	1.69	17.60	1.31
#4	1101-11-1	809	958	0.83	8.86	1.25
	9785-6-2	746	964	0.95	12.85	1.30

testing company, whereas the D-day tests were all done in the material laboratory of Civil Engineering Department of National Taiwan University (NTU). From the test observations, all concrete cylinders had increasing compressive strength until their failures without any softening. In addition, all the concrete cylinders were crushed accompanying with strong explosion in a brittle way. The results of the concrete cylinder tests can be found in Table 2.

High-yield strength steel is used for both of longitudinal ( $f_y = 685$  MPa) and transverse ( $f_y = 785$  MPa) reinforcements in all columns. The purposes of using high-yield strength stirrups are to provide good confinement for HSC core while keep the stirrup to remain elastic for cracks control. In addition, the stirrup spacing can be increased so that the constructability of RC members can be improved.

A slightly lower strength longitudinal bar than the stirrup is chosen in order to make the bar relatively easy to yield to achieve a ductile failure mode. A series of steel coupon tests has been conducted for both #4 and #8 bars. Each size of bars has three specimens. The bar stress versus strain relationships were obtained. Table 3 summarizes the averaged mechanical properties taken from the specimens.

### 3.3 Test variables

Three key parameters are investigated in this study, including: 1) the level of axial load; 2) the spacing of transverse reinforcement; and 3) the configuration of transverse reinforcement. The level of axial load is defined as the ratio between the applied constant axial compression and the column axial-load capacity  $P/P_0$ . The tests were carried out up to the failure of columns characterized by the loss of axial load capacity.

### 3.4 Instrumentations and test procedures

A total of 264 strain gauges were placed in each column to monitor the strains and yield state of the reinforcing bars at various locations. Among them, 36 strain gauges were placed in the longitudinal bars and the remaining for transverse bars. The strain gauges for longitudinal bars were located in three different regions, i.e. at the bottom, top, and middle of the column. Two levels of strain gauges were installed at each region to avoid possible damage during the construction of column specimens. Fig. 2 shows the detailed locations of the strain gauge.

To measure lateral displacement of the columns, two linear variable displacement transducers (LVDTs) were installed at the top and bottom footings. In order to find column axial displacement and displacement components, 12 optical sensors were placed at certain spacing along the column height and 4 optical sensors at the top and bottom footings as shown in Fig. 3a. All the optical sensors were supported by steel rods. The rods were passing through the column concrete core, extending from one side to the other side and tied to the vertical reinforcements prior to the pouring of concrete.

During the tests, columns put vertically with the top and bottom footings fixed at the cross beam and at the platen. The axial load was imposed by the vertical actuators to the bottom footing

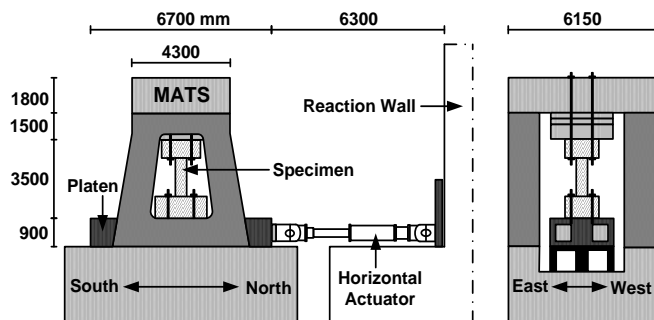


Fig. 4 Test setup



and keep to be constant along the test. The cyclically-increasing lateral load was given by the horizontal actuators to the top footing, imposing the double curvature to column. The drift ratios applied in these tests were 0.25, 0.375, 0.50, 0.75, 1, 1.5, 2, 3, 4, and 5% of drift radians, respectively. Each of drift ratios consists of three cycles. Fig. 3b illustrates the lateral loading protocol applied.

The lateral load was displacement controlled (loading rate = 0.4 mm/sec) and applied along the north and south directions as shown in Fig. 4. The north direction is considered as the positive direction for the lateral load or displacement. Through the procedures, axial load was applied first up to the target value following by lateral load. All the test data were stored in the predetermined steps. The concrete cracking and spalling were also marked and recorded.

## 4. Test results

### 4.1.1 Columns NRC-A1 and B1 under high-axial load

The first few cracks of specimens NRC-A1 and B1 were occurred at a drift ratio of 0.25% radian. The cracks observed in three different locations: at the very top and bottom four corners, and all around at the mid height of columns. At the top and bottom corners, the cracks spread diagonally. Meanwhile, the cracks at the mid-height propagated horizontally and vertically. These cracks caused concrete cover spalling in small part near the column mid-height of NRC-A1 and at the bottom corner of NRC-B1. When the drift reached 0.50% radian, a large portion of concrete cover in NRC-B1 spalled off, from top to lower half column height. Up to the third cycle 0.75% radian drift, crack at the bottom corner of NRC-A1 became wider and propagated diagonally. At this moment, most of concrete cover in NRC-B1 has been crushed on all sides, making the column into a severely damaged condition. Moreover, the vertical cracks also had already been developed in both of columns, extending from top to bottom. Stepping into the 1.0% radian drift, some vertical cracks more clearly appeared along the center of column. These vertical cracks caused the concrete cover of NRC-B1 spalled in a large portion, leading the column to fail. Meanwhile, for specimen NRC-A1, concrete cover spalled in large chunks when the drift comes to 1.5% radians. This put the column into a severely damaged condition and finally failed at the second cycle (Fig. 5a and 5c). Both of columns failed in the brittle manner, accompanied with concrete cover explosion and a loud of sound (Fig. 6a and 6c). As discussed, the vertical cracks were clearly established in both two columns due to the presence of high-axial load. These vertical cracks were never reported in the column tests using low-axial loads conducted by other researchers before.

### 4.1.2 Columns NRC-A2 and B2 under low-axial load

In contrast to columns under high-axial load, columns under low-axial load showed very different behaviors. In NRC-A2 and B2, there were no significant cracks up to the end of 0.75% radian drift, except some minor horizontal cracks. These cracks appeared at one-quarter of column height close to the top and bottom ends on all faces. At 1.0% radian drift, the diagonal cracks started to appear at the mid-height of column. Meanwhile, the vertical cracks developed in the top end of NRC-A2. When the drift of 1.5% radians was completed, all the top and bottom corners were crushed. Advanced to 2.0% radians drift, large vertical cracks appeared near the edges along the column height of NRC-A2. In the same time, the diagonal cracks and concrete cover spalling in NRC-B2 became more severe. At 3.0% radians drift, the diagonal cracks in both of columns

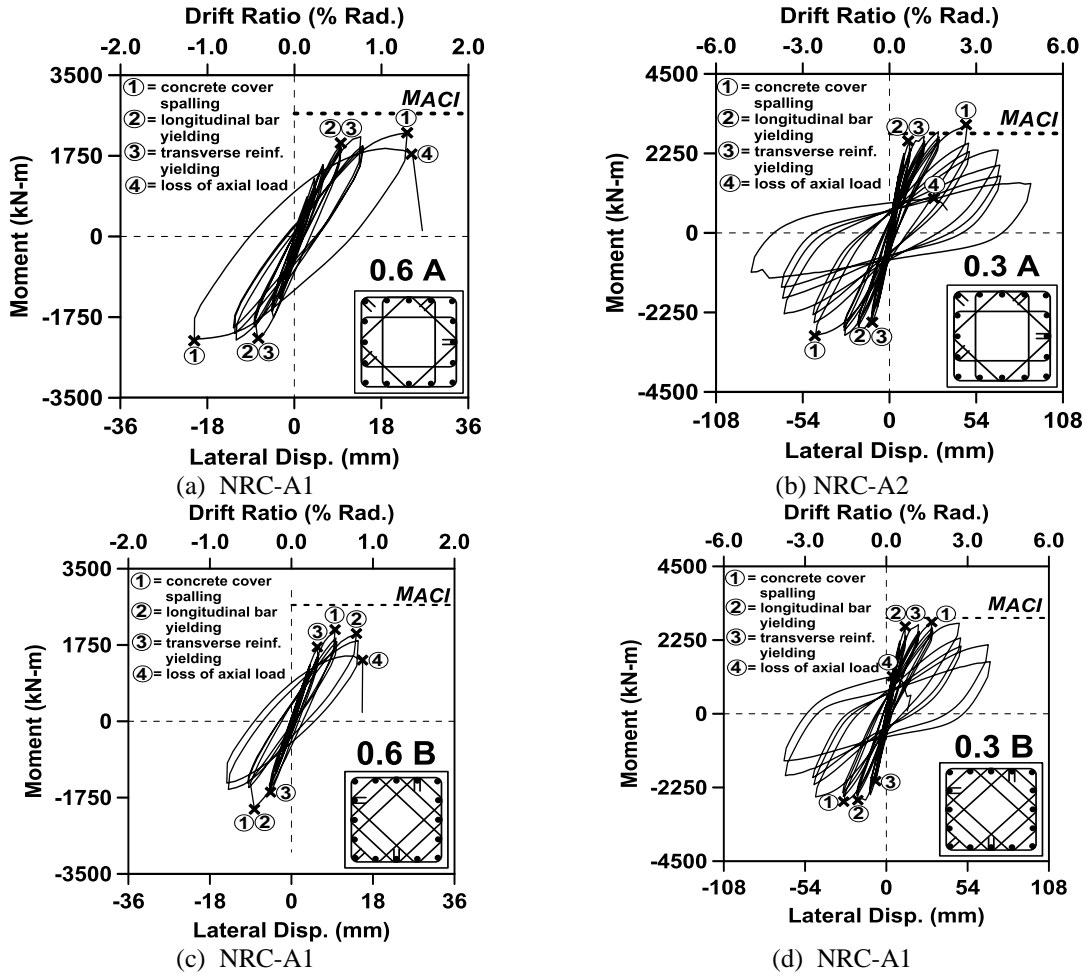


Fig. 5 Column moment versus lateral displacement relationships

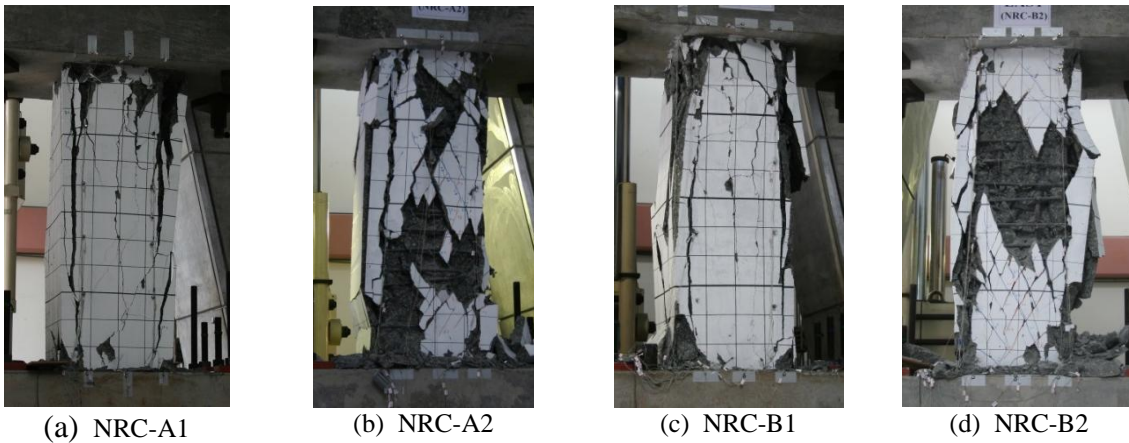


Fig. 6 Column failure modes

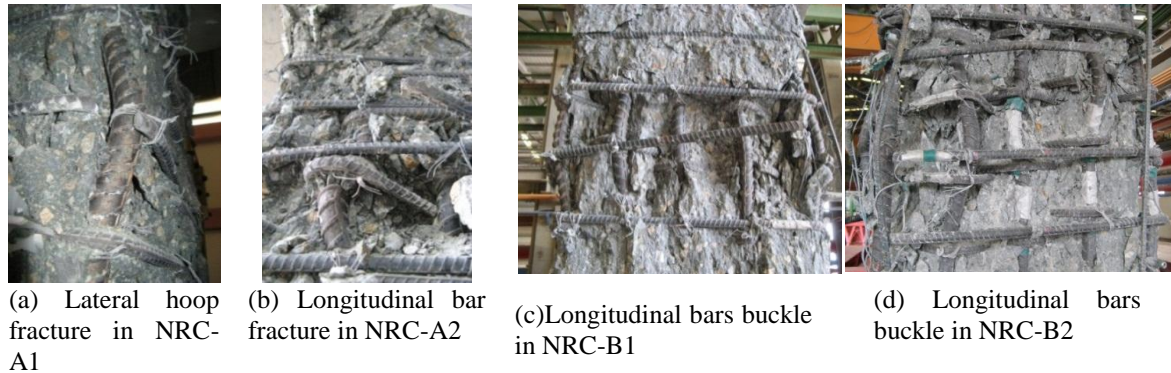


Fig. 7 Fracture and buckling of steel bars

Table 4 Summary of test results and prediction

Column	Moment, kN-m (kips-in.)			$\mu_{\Delta}$	$E_n$	$\delta_{ult}$ (%)
	$M_{test}$	$M_{ACI}$	$M_{test}/M_{ACI}$			
NRC-A1	2249	2668	0.84	3.3	12.3	1.2
NRC-A2	3013	2816	1.07	5.9	16.2	3.4
NRC-B1	2058	2520	0.82	2.5	9.0	0.9
NRC-B2	2770	2926	0.95	5.8	14.6	3.1

started to connect each other. As a result, several vertical cracks occurred in the center of column, propagated from the top to bottom ends. As cyclic lateral displacement increased, these vertical cracks became more widely opened. Stepping into 4% radians drift, concrete cover began to spall extensively and up to the completion of third cycle, concrete cover crushed completely on all faces. These evidences made the column NRC-B2 failed at the third cycle under the positive lateral force. Slightly better, column NRC-A2 failed at the second cycle of 5.0% radians drift under the negative lateral force (Fig. 6b and 6d). At the time of failure, neither concrete cover explosion nor a loud of sound was experienced as the case of columns under high-axial load. This indicates that NRC-A2 and B2 failed in a ductile manner (Fig. 5b and 5d).

#### 4.1.3 Post-experimental investigation

The post-experimental investigation indicated that the presence of high-axial load has very significant effects on the column failure mode and the maximum drift ratio achieved. All HSM column failures were identified with the longitudinal bars buckled or lateral hoops fractured. The longitudinal bars buckling occurred mostly at the top and bottom ends of column corner. The buckling of the longitudinal bars often followed by the fracture of the transverse reinforcement hoops (Fig. 7).

In case of NRC-A1, a total of nine longitudinal bars were buckled and ten lateral hoops were fractured. Four of them are corner bars and the remaining are near-corner bars (Fig. 7a). Most of buckling bars are located in one-quarter height of both top and bottom ends. In NRC-B1, thirteen longitudinal bars were found buckle in all sides. In addition, three other longitudinal bars and more than ten lateral hoops were fractured (Fig. 7c).

As exhibited by columns A1 and B1, column A2 and B2 also failed with longitudinal bars buckled and lateral hoops fractured. The only difference is that A2 and B2 failed at the high drift

ratio of 4.0% radians or higher. In such high drift, most of the vertical bars were buckled. More than twenty different locations of longitudinal bars buckled and lateral hoops fractured in A2 (Fig. 7b).

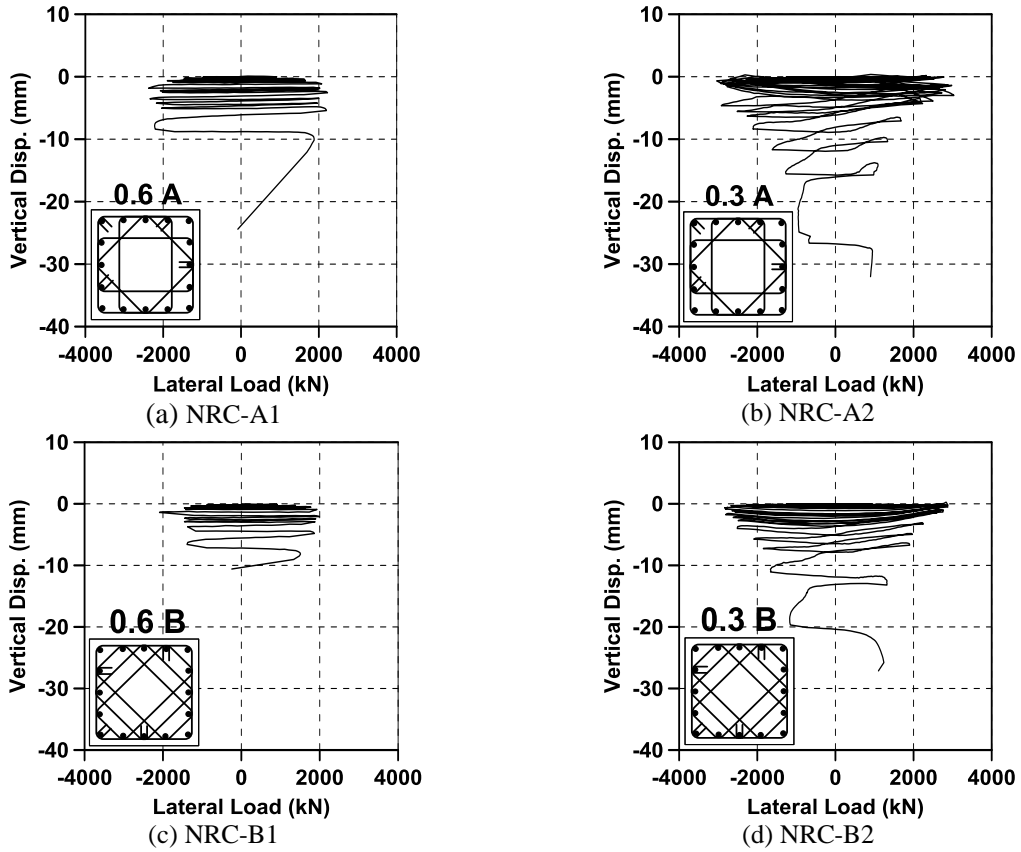
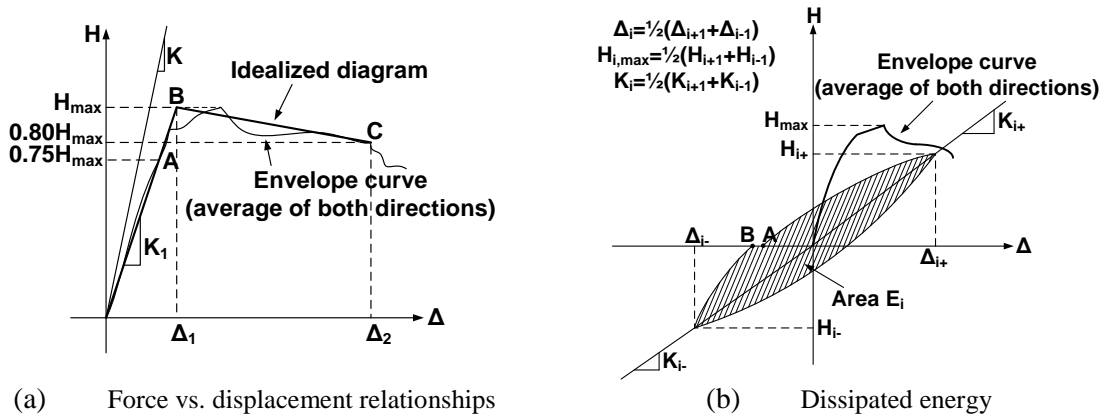


Fig. 8 Illustration for ductility and dissipated energy calculation



(a) Force vs. displacement relationships

(b) Dissipated energy

Fig. 9 Illustration for ductility and dissipated energy calculation

Similarly, longitudinal bars buckled and lateral hoops fractured also found in NRC-B2 (Fig. 7d). At the end of all column tests, none of the 135-degree hooks were found opened.

In this test series, hoop fracture occurred in all four HSM columns. This is the anticipated consequence as HSC requires much higher lateral confinement pressure than the normal-strength concrete does. This kind of column hoop failure mode has also been reported in other studies using HSM (Li and Park, 2004). Nevertheless, this failure mode was less-frequently observed in column tests using normal strength hoops. Typical failure modes of normal strength hoops are yielding of the bars or opening of the hooks. Since the high-strength hoops were fractured in this study, it is reasonable to assume that the hoops have reached the yield strain. This suggests that the confinement provided by the high-yield strength steel hoops has been achieved. Research conducted by Razvi and Saatcioglu (1994) also indicated that using high-yield strength steel for transverse reinforcement was fully effective in confining HSC. Increasing ductility up to 2.5 times has been obtained when the normal-strength hoops were replaced by high-yield strength stirrups.

#### 4.2 Cyclic force versus displacement relationships

The moment versus lateral displacement relationships of all HSM columns are shown in Fig. 5. The moment capacity based on ACI-318 provision is included as shown by the dashed lines. Currently, there is no agreement between the researchers to calculate the moment capacity of HSC or HSM columns (Hwang and Yun 2004). In this study, a rectangular stress block defined by ACI 318-11 Section 10.2.7 was adopted in calculating the moment capacity. Since this section does not limited the use of equivalent rectangular stress block to any specific concrete compressive strength, therefore the  $\alpha_1 = 0.85$  and  $\beta_1 = 0.65$  are applied. The actual concrete and steel bars strengths were employed in the calculation. The P-Delta moment is included in the bending responses shown in Fig. 5. The occurrence of certain key instances such as concrete cover spalling, transverse reinforcement yielding, longitudinal reinforcement yielding, and loss of axial load capacity are indicated in the figures.

The general relationships between the lateral load and lateral displacement of HSM columns under low-axial load typically follow the steps reported by Xiao and Yun (2002) for HSC columns. These three stages include: 1. initial stage, which is accommodated by the participation of both of unconfined concrete cover and confined concrete core, 2. stable behavior, mainly marking with concrete cover cracking, longitudinal steel yielding, and concrete core straining, and 3. final failure, when the column loss its axial and or lateral capacity. In addition, the maximum HSC column lateral strength is reported to appear shortly before the unconfined concrete cover crushed and spalled off.

According to the test results, columns under low-axial load exhibited a better response in terms of lateral strength and deformation capacities than those showed by columns under high-axial load. NRC-A2 and NRC-B2 behaved in a stable manner up to 5.0% and 4.0% radians drift. The maximum lateral loads achieved are 3038 kN and 2883 kN, when the lateral displacements were 27.8mm and 21.4mm, respectively. In contrast, NRC-A1 and NRC-B1 behaved stably only up to 1.5% and 1.0% radians drift. Afterwards, the columns degraded suddenly heading to failure. The maximum lateral loads achieved are 2374 kN and 2161 kN, when the corresponding lateral displacements are 8.1mm and 9.6mm. These results are apparently due to the presence of the high-axial load which significantly influences the column lateral strength and deformation capacities. Indeed as reported by Xiao and Yun (2008), the maximum lateral load of all four HSM columns

was attained shortly before concrete cover crushing and spalling. The vertical displacement of HSM columns was also recorded during the test. Fig. 8 shows the lateral load versus vertical displacement relationships.

#### 4.3 Ductility and energy dissipation

The seismic performance of structural members can be described in terms of ductility and energy dissipation capacities. According to most of the seismic force specifications, ductility capacity is considered as the key factor directly affecting the reduction factor used in calculating the base shear for long period structures. Meanwhile, the energy dissipation capacity is an important parameter to design short-period structures or structures subjected to a long duration earthquake (Newmark and Hall 1980). In this paper, the displacement ductility and normalized energy dissipation capacities are chosen as the column performance indicators for rational comparison purposes.

Since the behavior of reinforced concrete structures is not elastic-perfectly plastic, it has been the general practice to use an idealized lateral displacement versus lateral load relationship to define the displacement ductility parameter (Fig. 9a). The bilinear response was chosen as the idealized relationship consisting of the elastic and post-elastic branches. The elastic response is defined as a secant line at 75% of maximum lateral load to the actual experimental response (point A) and continued up to the maximum lateral load (point B). The corresponding displacement at the maximum lateral load is assigned as the yield displacement  $\Delta_1$ . The actual experimental response is an average envelope curve of the actual positive and negative load responses. Meanwhile, the post-elastic response is a linear response initiated from the maximum lateral load (point B) up to the column failure where lateral strength reduced to 80% of the peak lateral load (point C). The displacement associated with the column failure point is defined such that the area under the real experimental curve and the idealized diagram are the same. The displacement at the column failure (point C) then is appointed as the maximum displacement  $\Delta_2$ . In this manner, the equal energy criteria can be met (Bayrak and Sheikh 1997; Legeron and Paultre 2000; Hwang and Yun 2004; Ahn and Shin 2007).

Thus, the column displacement ductility  $\mu_\Delta$  can be computed from:

$$\mu_\Delta = \Delta_2 / \Delta_1 \quad (1)$$

Columns can be considered ductile if the displacement ductility within the range of 4 to 6 (Legeron and Paultre 2000).

The total column energy dissipation during the test is defined as a cumulative dissipated energy from each cycle  $E_i$  up to the column failure. The hatched area in Fig. 9b illustrates the energy dissipation of a loading cycle. The energy dissipation of each cycle  $E_i$  can be computed from:

$$E_i = \int_A^B H d\Delta \quad (2)$$

Thus, the total energy dissipation of the column is calculated by:

$$E_{hyst} = \sum_{i=1}^n E_i \quad (3)$$

where  $n$  is the total number of cycles up to the column failure. For comparison purposes, the energy dissipation must be normalized as:

$$E_N = \frac{1}{H_{max}\Delta_1} \sum_{i=1}^n E_i \quad (4)$$

where  $E_N$  is the normalized energy dissipation (Bayrak and Sheikh 1997; Legeron and Paultre 2000; Hwang and Yun 2004, Caballero-Morrison, *et al.* 2012). The displacement ductility and energy dissipation of all HSM columns is given in Table 4.

#### 4.4 Displacement components

The column total lateral displacement is the contribution of three major deformation components: (1) flexure, (2) slip, and (3) shear deformations (Sezen 2000; Sezen and Moehle 2006). In order to measure the percentage contribution of three major deformation components, a number of optical sensors were attached along the column height. The sensors were arranged such that each four sensors formed a rectangular segment as shown in Fig. 3. All the deformation components can be computed as described in the following.

Fig. 10 illustrates the parameters adopted in calculating the column flexural deformation. The column flexure deformation is calculated by integrating the flexural curvatures along the column height:

$$\Delta_{flexure} = \int_0^L \phi x dx \quad (5a)$$

$$\Delta_{flexure} = \sum_{i=1}^n \theta_i d_i = \sum_{i=1}^n \frac{\delta_{l,i} - \delta_{r,i}}{b_i} d_i \quad (5b)$$

where  $\theta_i$  = the average rotation angle for the  $i^{th}$  segment,  $d_i$  = the vertical distance from the center of the segment to the column top,  $b_i$  = the averaged width of the  $i^{th}$  segment, and  $\delta_{l,i}$  and  $\delta_{r,i}$  are the relative vertical displacement measured from the left and right optical sensors of the segment. Here,  $n$  is total number of segments.

The shear deformation in a segment is computed from:

$$\gamma_i = \frac{\sqrt{a^2 + b^2}}{2ab} (\delta_1 + \delta_2) \quad (6a)$$

$$\Delta_{shear} = \sum_{i=1}^n \gamma_i \times b_i \quad (6b)$$

where  $a$  = the average height of the segment,  $\delta_1$  and  $\delta_2$  = the change of the diagonal length in the segment, and  $\gamma$  = the drift of the segment (Fig 11a). Column total shear deformation is obtained by summing the shear deformation of all segments along the column height.

The slip deformation is computed from summing the column top and bottom slip angles time the half column height using the following three equations:

$$\theta_{slip-top} = (\phi_{T-top} - \phi_{max-top}) \times a_{top} \quad (7a)$$

$$\theta_{slip-bot} = (\phi_{T-bot} - \phi_{max-bot}) \times a_{bot} \quad (7b)$$

$$\Delta_{slip} = (\theta_{slip-top} + \theta_{slip-bot}) \times 0.5H \quad (7c)$$

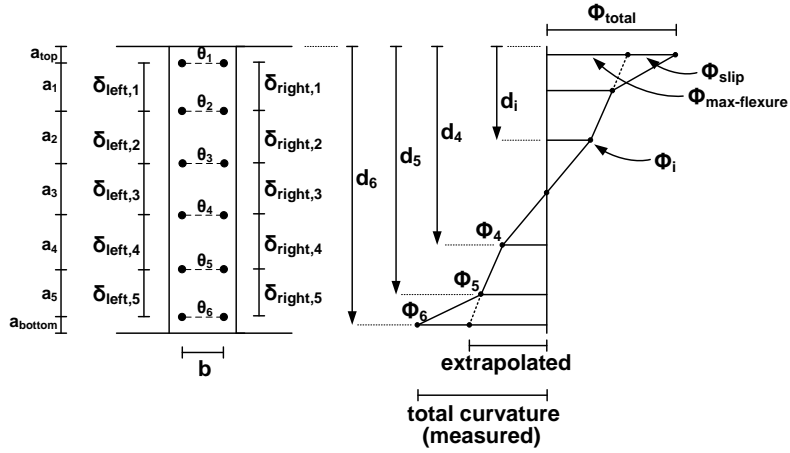
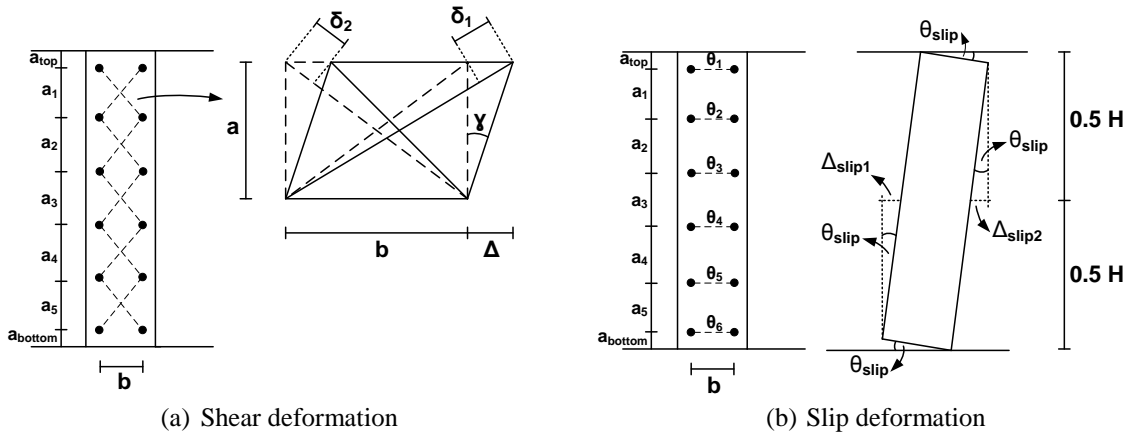


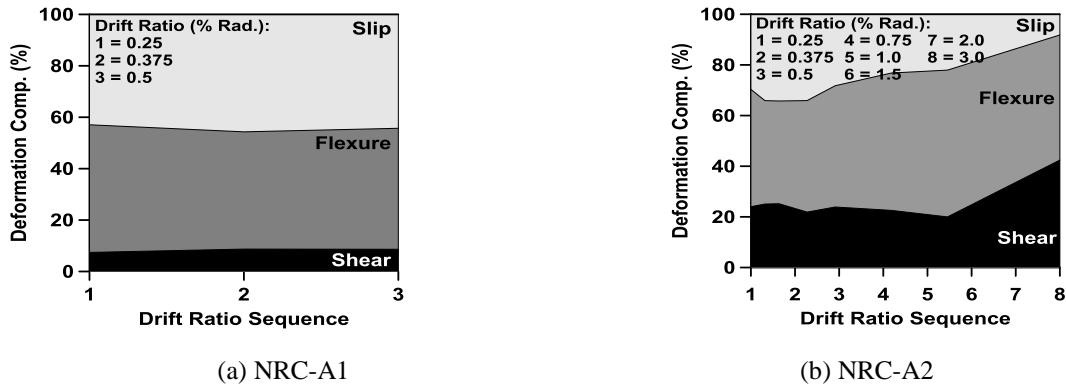
Fig. 10 Column flexural deformation parameters



(a) Shear deformation

(b) Slip deformation

Fig. 11 Column shear deformation parameters



(a) NRC-A1

(b) NRC-A2

Fig. 12 The percentage of column deformation components

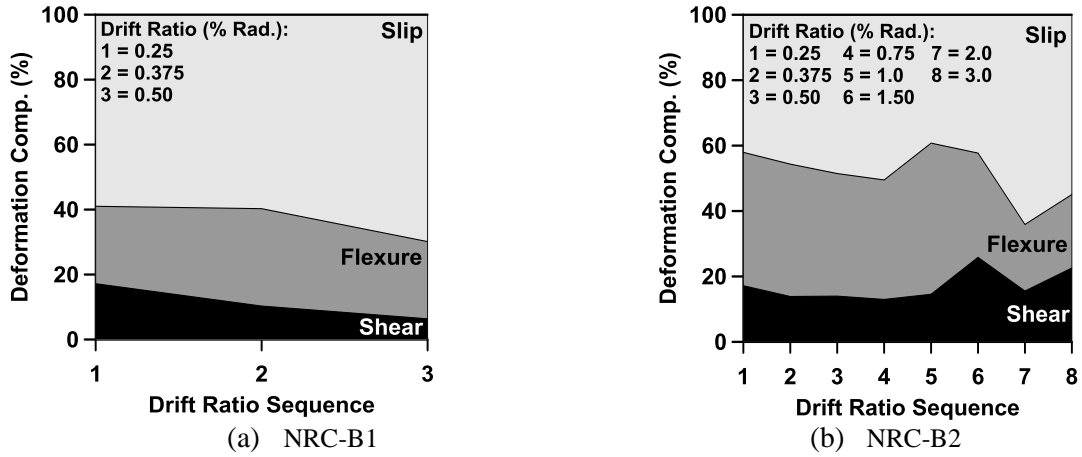


Fig. 12 Continued

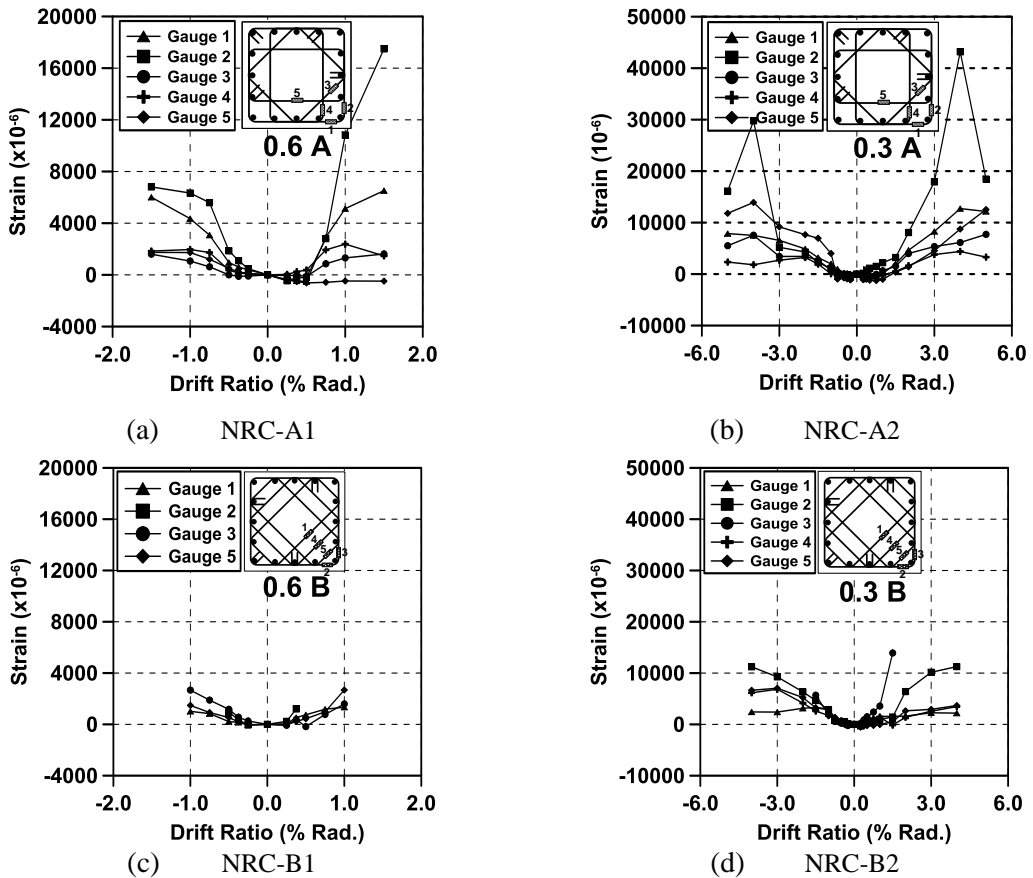


Fig. 13 Sample of transverse reinforcement strains at various drift levels

where  $\phi_{T-top}$ ,  $\phi_{T-bot}$  = the total curvature at the top or bottom most segment,  $\phi_{max-top}$ ,  $\phi_{max-bot}$  = maximum extrapolated flexural curvature at the top or bottom most segment,  $a_{top}$ ,  $a_{bot}$  = the average of vertical distance at the outermost segment, and  $H$  = the column height (Fig 11b). Due to the slip of the longitudinal bars in the column top and bottom ends, it is assumed that the maximum average curvature occurred at the outermost segments at the top and bottom ends.

Since the sensors were adhered to the concrete surface, any cracks or spalling of the concrete could cause serious problems to the sensor readings. Thus, cracks and concrete spalling often led to some sensor readings disturbed and even lost completely. Consequently, the data were not fully available for the entire columns test. The valid data were recorded up to 0.5% radian drift for columns under high-axial load while for columns under low-axial load up to 1.5% radians drift. In quantifying the displacement component contributions, the respective displacement components are divided by the total lateral displacement and multiplied by 100%. Fig. 12 shows the percentage of displacement components to the peak lateral displacement at various drift levels.

As shown in Fig. 12, shear deformation contribution in columns under high-axial load (NRC-A1 and B1) was relatively smaller compare to flexure and slip deformations. At the various drift levels, it only contributes less than 10% while flexure and slip deformations contribute approximately 20-50% and 40-70% of the total column lateral displacements, respectively. However, it appears in columns under low-axial load (NRC-A2 and B2) that shear deformation contribution increased up to approximately 10-25% of the total column lateral displacements. The flexure and slip deformation contributions in these columns were about 30-50% and 20-50%, respectively.

#### 4.5 Transverse reinforcement strain distributions

Fig. 13 shows the typical strain distributions of the transverse reinforcement for all HSM columns at the critical region near the top and bottom column ends. The actual yield strain of these reinforcements was more than 4,000 microstrains. According to the test results, it appears that the first yield of lateral hoops in columns under high-axial load of NRC-A1 and B1 took place at a relatively small drift ratio of 0.75% radian drift. More than six lateral hoops of these columns reached yielding at this drift ratio. Meanwhile, columns under low-axial load NRC-A2 and B2 obtained their first yield at 1.5% radians drift. At that same drift, more than 10 lateral hoops in the critical region hoops of NRC-A2 and B2 were yield. The early yield of lateral hoops in NRC-A1 and B1 was assumed due to the presence of the high-axial load. After the cover spalled off, the lateral hoop allowed the concrete core to sustain an increased compressive stress and restrained the longitudinal bars from buckling. However, due to the increased concrete core compression pressure, a higher hoop tensile strain will also be developed. It is evidenced from the aforementioned test results that the presence of high-axial load in NRC-A1 and B1 has affected the lateral hoops to yield earlier than the case in NRC-A2 and B2.

## 5. Discussions

The three test parameters are discussed in this section: (1) effects of axial load applied; (2) spacing; and (3) configuration of the transverse reinforcement.

### 5.1 Effects of axial load applied

The effects of axial load applied on the HSM column responses can be investigated from the two counterparts of column, NRC-A1 and B1; and NRC-A2 and B2. The axial loads applied to the columns were  $0.60P_0$  for NRC-A1 and B1; and  $0.30P_0$  for NRC-A2 and B2. The experimental results showed that columns under low axial-load had better responses than those shown by columns under high-axial load. The responses including column flexural strength and maximum drift achieved as well as column ductility and energy dissipated.

As the experimental results show, the maximum flexural strength achieved by NRC-A2 and B2 are approximately 34% and 35% larger than those achieved by NRC-A1 and B1. The maximum flexural strength of NRC-A2 and B2 were 3013 kN and 2770 kN while NRC-A1 and B1 were only 2249 kN and 2058 kN. Similarly, the displacement ductility  $\mu_\Delta$  attained by NRC-A2 and B2 are significantly larger than those by NRC-A1 and B1 for about 80% and 130%. The displacement ductility  $\mu_\Delta$  calculated from NRC-A2 and B2 are 5.9 and 5.8, meanwhile, NRC-A1 and NRC-B1 only reached 3.3 and 2.5. A similar trending was also found for maximum drift and energy dissipation gained. NRC-A2 and B2 attained their maximum drift of 4.9% and 3.8% and is much higher than 1.4% and 0.9% attained by NRC-A1 and NRC. The energy dissipated by NRC-A2 and B2 are also larger than those by NRC-A1 and B1 at approximately 37% and 62%. All these results indicating that high-axial load, however, affected the performance of column significantly and caused degradation in column strength and lateral deformation capacity.

The employment of ACI-318 to calculate the moment capacity of HSM columns has resulted in overestimated prediction, particularly for columns under high-axial load. Over estimations approximately 19% and 22% have been made for NRC-A1 and B1. Meanwhile, there was no agreement for column under low-axial load. Slightly over conservative prediction has been made for NRC-B2 for about 6%, whereas less prediction for about 7% has been made for NRC-A2. These results suggest that further researches are required to establish a more accurate method to compute the moment capacity for HSM columns. The ACI-318 may not be suitable for estimating the moment capacity of HSM columns because it is developed from the researches on normal strength concrete.

### 5.2 Effects of spacing and configuration of transverse reinforcement

The effects of transverse reinforcement spacing and configuration can be assessed from the column counterparts of NRC-A1 and A2 as well as NRC-B1 and B2. Transverse reinforcement spacing of 105mm with type A configuration was used by NRC-A1 and A2. Meanwhile, NRC-B1 and B2 used of 120mm spacing with type B configuration.

The test results indicate that columns using closer transverse reinforcement spacing or type A had slightly better responses compare to columns with higher spacing or type B. Maximum shear strength gained by NRC-A1 is 2499 kN, which is 9.3% more than 2286 kN by NRC-B1. In similar, maximum shear strength obtained by NRC-A2 is 3348 kN, which is 8.8% larger than obtained by NRC-B2 of 3078 kN. Furthermore, the displacement ductility  $\mu_\Delta$  achieved by NRC-A1 is 28% higher than achieved by NRC-B1 while NRC-A2 only have 2% higher than NRC-B2. The same tendency was found for the maximum drift and energy dissipated by the HSM columns. NRC-A1 has 41% larger of maximum drift capacity than NRC-B1 while NRC-A2 only has 9% larger than NRC-B2. The dissipated energy computed from NRC-A1 and A2 is also larger than obtained by

NRC-B1 and B2 for about 37% and 11%, respectively. As the results show, it is very clear that smaller transverse reinforcement spacing led to increase significantly of HSM column capacities, particularly for columns under high-axial load.

## 6. Conclusions

Based on the results of this experimental investigation, the conclusions are drawn as follows:

- Under low-axial load, HSM columns using minimum transverse reinforcement spacing as required by ACI 318 provision perform satisfactorily.
- The 135-degree hooks provide a sufficient confinement for earthquake resistant design of HSM columns.
- The behaviors and responses of HSM columns are not significantly affected by the transverse reinforcement configuration.
- The moment capacity of HSM columns under high-axial load is overestimated by the ACI-318 provision since it is developed from researches on normal strength concrete.

## Acknowledgments

The authors would like to thank National Science Council of Republic of China for the funding. The experimental work was performed in the National Center for Research on Earthquake Engineering (NCREE), Taipei. Technical assistance from NCREE staff, particularly Dr. K.C. Lin and Mr. S.J. Jhuang is very much appreciated. Assistance from many graduate students is very gratefully acknowledged.

## References

- ACI Committee 318 (2011), *Building Code Requirements for Structural Concrete (ACI-318-11) and Commentary*, American Concrete Institute, Farmington Hills, MI, USA.
- ACI Committee 363 (1992, Reapproved 1997), *State-of-the-Art Report on High Strength Concrete (ACI 363R-92)*, American Concrete Institute, Farmington Hills, MI, USA.
- Ahn, J.M. and Shin, S.W. (2007), "An evaluation of ductility of high-strength reinforced concrete columns subjected to reversed cyclic loads under axial compression", *Mag. Concrete Res.* **59**(1), 29-44.
- Ashtiani, M.S., Scott, A.N. and Dhakal, R.P. (2013), "Mechanical and fresh properties of high-strength self-compacting concrete containing class C fly ash", *Construct. Build. Mater.*, **47**, 1217-1224.
- Bayrak, O. and Sheikh, S.A. (1997), "High-strength concrete columns under simulated earthquake loading", *ACI Struct. J.*, **94**(6), 708-722.
- Caballero-Morrison, K.E., Bonet, J.L, Navarro-Gregori, and Marti-Vargas, J.R. (2012), "Behaviour of steel-fibre-reinforced normal-strength concrete slender columns under cyclic loading", *Eng. Struct.*, **39**, 162-175.
- Elwood, K.J., Maffei, J., Riedere, K.A. and Telleen, K. (2009), "Improving column confinement-Part 1: assessment of design provision", *Concrete International*, November.
- Ho, J.C.M. and Luo, L. (2012), "Uni-axial behaviour of normal-strength concrete-filled-steel-tube columns with external confinement", *Earthq. Struct.*, **3**(6), 889-910.

- Hwang, S.K. and Yun, H.D. (2004), "Effect of transverse reinforcement on flexural behaviour of high-strength concrete columns", *Eng. Struct.*, **26**, 1-12.
- Hwang, S.K., Yun, H.D., Park, W.S. and Han, B.C. (2005), "Seismic performance of high-strength concrete columns", *Mag. Concrete Res.*, **57**(5), 247-260.
- Kawai, T. (2007), "State-of-the-art report on high-strength concrete in Japan -recent developments and applications-", [http://www.jsce.or.jp/committee/concrete/e/newsletter/newsletter05/7-Vietnam%20Joint%20Seminar%20\(Kawai\).pdf](http://www.jsce.or.jp/committee/concrete/e/newsletter/newsletter05/7-Vietnam%20Joint%20Seminar%20(Kawai).pdf)
- Legeron, F. and Paultre, P. (2000), "Behavior of high-strength columns under cyclic flexure and constant axial load", *ACI Struct. J.*, **97**(4), 591-601.
- Lepage, A., Tavallali, H., Pujol, S. and Rautenberg, J. (2008), "Towards earthquake-resistant concrete structures with ultra high-strength steel reinforcement", *The 14<sup>th</sup> World Conference on Earthquake Engineering, Beijing*, October.
- Li, B. and Park, R. (2004), "Confining reinforcement for high-strength columns", *ACI Struct. J.*, **101**(3), 314-324.
- Newmark, N.M. and Hall, W.J. (1980), *Earthquake Spectra and Design*, Earthquake Engineering Research Institute, Berkeley, California, USA
- Rashid, M.A., Mansur, M.A. and Paramasivam, P. (2002), "Correlation between mechanical properties of high-strength concrete", *ASCE J. Mater. Civil Eng.*, **14**, (3), 230-238.
- Razvi, S.R., and Saatcioglu, M (1994), "Strength and deformability of confined high-strength concrete columns", *ACI Struct. J.*, **91**(6), 1-10.
- Sezen (2000), "Seismic behavior and modeling of reinforced concrete building columns", Ph.D. Dissertation, University of California, Berkeley.
- Sezen, H. and Moehle, J.P. (2006), "Seismic test of concrete columns with light transverse reinforcement", *ACI Struct. J.*, **103**(6), 842-849.
- Xiao, X., Guan, F.L. and Yan, S. (2008), "Use of ultra-high-strength bars for rectangular high-strength concrete frame columns", *Mag. Concrete Res.*, **60**(4), 253-259.
- Xiao, Y. and Yun, H.W. (2002), "Experimental studies on full-scale high-strength concrete columns", *ACI Struct. J.*, **99**(2), 129-207.
- Zhou, K.J.H., Ho, J.C.M. and Su, R.K.L. (2010), "Normalised rotation capacity for deformability evaluation of high-performance concrete beams", *Earthq. Struct.*, **1**(3), 269-287.